Eulerian calculations of wave breaking and multi-valued solutions in a traveling wave tube

J.G. Wöhlbier,[1] S. Jin,[2] and S. Sengele[3]

[1]Los Alamos National Laboratory, ISR-6, Radio Frequency and Accelerator Physics, Los Alamos, NM 87545, USA
[2]Department of Mathematics, University of Wisconsin, Madison, WI 53706, USA
[3]Department of Electrical and Computer Engineering,
University of Wisconsin, Madison, WI 53706, USA

The traveling wave tube is an electron beam device that works on a similar principle to the beam-plasma instability, where the background plasma is replaced by an electromagnetic waveguiding structure. The nonlinear evolution of the instability includes wave breaking and the formation of multi-valued solutions, and conventionally these solutions have been computed using Lagrangian techniques. Recently, an Eulerian method for computing multi-valued solutions was developed in the context of geometrical optics, and has been applied to the klystron, a relative of the traveling wave tube. In this paper we apply the Eulerian technique to solve a traveling wave tube model and compare the results to a Lagrangian technique. The results are found to be in good qualitative agreement with small quantitative differences that are attributed to the numerical methods.

I. INTRODUCTION

It is well known that solutions to nonlinear hyperbolic wave equations can exhibit "steepening," and can "break" in a finite time. Most commonly the physical situations being modeled dictate that shock formation occurs at the breaking point. However, it has long been acknowledged that another interpretation of the breaking event is the formation of "multi-valued solutions" [1], although methods for computing multi-valued solutions have not been pursued nearly to the extent that shock formation and shock capturing techniques have. Recently an Eulerian technique for computing multi-valued solutions was developed in the context of geometrical optics [2–4] and the semi-classical limit of the linear Schrödinger equation [5]. In [6] this technique is applied to the Euler-Poisson equations which may be used to model, among other systems, nonlinear electron beam evolution in klystron amplifiers. In this paper we apply the technique to a relative of the klystron, the traveling wave tube (TWT).

In plasma physics wave breaking in nonlinear plasma waves was first discussed by Dawson [7]. There is a substantial body of literature discussing wave breaking in nonlinear plasma waves as relevant to plasma heating, plasma accelerators, laser fusion, general laser-plasma interactions, and electron beams. Restricting our interest to the cold plasma wave breaking literature since it is most relevant to this paper, plasma wave breaking is treated in, for example, [8–11], and electron beams are treated in [12]. In [9, 10] no attempts are made to do calculations beyond the point of wave breaking. Rather, the wave amplitude for which wave breaking sets in is considered a limit for having a nonlinear plasma wave, since they were considering cases where wave breaking lead to a wave damping. Calculations beyond wave breaking for cold plasmas are performed using Lagrangian coordinates [8, 11].

Nordsieck's seminal TWT work [13] addressed wave breaking six years prior to Dawson [7], and pointed out that "electrons overtake one another at or even considerably before the point along the tube where the limiting power level is obtained," i.e., the solution breaks and becomes multi-valued. To address this problem Nordsieck used a Lagrangian electron beam description where the fluid element characteristics were allowed to cross and the solutions were allowed to become "multi-valued." The use of a Lagrangian electron beam description has become the standard in microwave vacuum electronics so that multi-valued solutions that form after "electron overtaking" are properly computed.

More generally the physics of a TWT is an example of a convective instability in a non-neutral plasma. It has been observed that "in the small cold beam limit, the equations governing the evolution of the beam-plasma instability are mathematically identical to those describing the traveling wave tube" [14]. Therefore, while we consider in this paper a TWT specifically, the model equations may be considered a prototype for more general plasma physics problems since they are related to the Vlasov-Poisson and Vlasov-Maxwell systems [15]. Eulerian techniques for computing such instabilities may be desirable in 1d when rays diverge, or in multiple dimensions, when Lagrangian meshes would be entangled due to crossing characteristics. A TWT may be modeled in 3d by the Vlasov-Maxwell system, and may provide another important prototype for Eulerian calculations of multi-valued solutions relevant to plasmas [15] in multiple dimensions [16].

In this paper we extend our work in [6] by considering a TWT model that has an additional wave equation beyond the model used for the klystron. In Sec. II we give a brief description of TWT physics and describe the model equations. We give the moment system that allows calculation of multi-valued solutions, and describe how the calculations are done. In Sec. III we present computational results for a TWT that is found in the litera-

ture [17, 18] using the multi-phase (multi-value) Eulerian method as well as a Lagrangian technique for comparison. Section IV concludes the paper. There are two appendices providing details regarding normalizations and the Lagrangian formulation.

II. MODEL EQUATIONS

A TWT is a microwave amplifier commonly used in telecommunications and electronic countermeasure systems. The source of energy for amplification of the microwaves is an electron beam that passes in close proximity to the electromagnetic waveguiding structure. A schematic showing the placement of the electron beam relative to a helix waveguide in a TWT is given in Fig. 1.
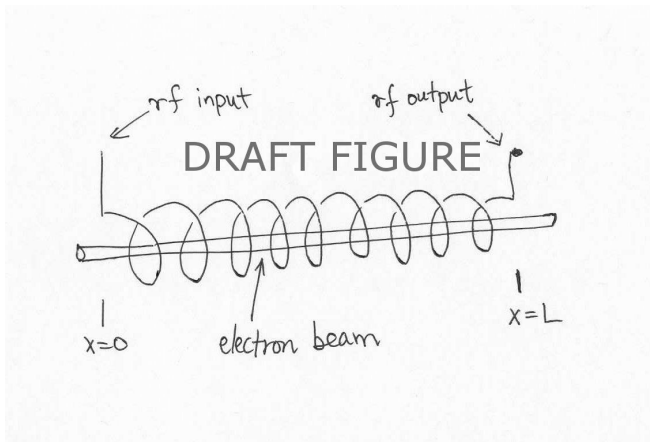

FIG. 1: (Color online) Schematic of helix TWT.

Typically the electron beam enters the helix unmodulated, i.e., with no density or velocity perturbations, into the same end as the input microwave signal and traveling approximately velocity synchronous with the microwave signal ("wave"). The axially directed electric fields provide accelerating and decelerating fields on the electrons, with a particular electron being accelerated or decelerated depending on where it sits in the phase of the wave. Slowing down and speeding up of the charges results in convecting, growing density bunches. The bunches form primarily in the decelerating phases of the wave, and hence the electrons give their energy up to the wave as they are decelerated. As a result of the energy exchange process the wave grows exponentially along the length of the amplifier. For sufficient levels of acceleration and deceleration electrons can pass by, or "overtake," electrons that were initially ahead of them. This is the point of wave breaking, and beyond this point velocity and density solutions become multi-valued.

A normalized set of TWT equations (see Appendix A) that reproduce the classic linear dispersion relation [19, 20] are

$$\frac{\partial V}{\partial x} + \frac{1}{v_{\text{ph}}} * \frac{\partial V}{\partial t} = C^3 * \frac{\partial \rho}{\partial t} \tag{1}$$

$$\frac{\partial E}{\partial x} = \rho - 1 \tag{2}$$

$$\frac{\partial \rho}{\partial t} + \frac{\partial}{\partial x}(\rho u) = 0 \tag{3}$$

$$\frac{\partial}{\partial t}(\rho u) + \frac{\partial}{\partial x}(\rho u^2) = \rho \left(-\frac{\partial V}{\partial x} + R * E \right) \tag{4}$$

where $*$ denotes convolution. In (1)–(4) V is the circuit voltage (microwave field), E is the coulomb space charge field, ρ is the beam charge density, u is the beam velocity, $1/v_{\text{ph}}$ is the inverse Fourier transform of the frequency dependent function $1/\tilde{v}_{\text{ph}}(\omega)$ where $\tilde{v}_{\text{ph}}(\omega)$ is the cold circuit phase velocity, C^3 is the inverse Fourier transform of the frequency dependent Pierce gain parameter [19] $\tilde{C}^3(\omega)$, R is the inverse Fourier transform of the frequency dependent space charge reduction factor $\tilde{R}(\omega)$, t is time, and x is distance along the TWT.

For the TWT one equation is added to the Euler-Poisson system as found in the klystron [6]. The additional equation is for the circuit voltage wave evolution as forced by the beam charge density, and the circuit voltage also appears as a forcing term in the momentum equation (4). Furthermore, the convolutions in (1) and (4) account for the frequency dependence of the circuit parameters. The frequency dependence acts as filter in that only the frequencies of the input signal with the right combinations of parameters grow exponentially. This filtering is critical in that the density singularities which form when the solution becomes multi-valued should not be allowed to manifest in the circuit field.

Direct application of a finite difference scheme to Eqs. (1)–(4) will not predict formation of multi-valued solutions; if Eqs. (1)–(4) are converted to Lagrangian coordinates (see Appendix B) they do predict formation of multi-valued solutions. To arrive at an Eulerian technique that predicts the multi-valued solutions one starts with the Vlasov equation coupled to Poisson's equation (2) and the circuit equation (1), and derives moment equations from the Vlasov equation using an initial distribution that is a delta function in velocity (see Appendix A). Since the solution to the distribution in the "Vlasov-TWT" system remains a delta function in velocity, the moment hierarchy may be closed exactly [5, 6].

Here we will simply state the moment system and refer the reader to [5, 6] for technical details such as the moment closure and numerical methods. For a solution with N values of velocity and density we need $2N$ moments. This will result in an invertible mapping between the moments and the densities and velocities [5]. The

moment system is

$$\frac{\partial V}{\partial x} + \frac{1}{v_{\text{ph}}} * \frac{\partial V}{\partial t} = C^3 * \frac{\partial m_0}{\partial t} \tag{5}$$

$$\frac{\partial E}{\partial x} = m_0 - 1 \tag{6}$$

$$\frac{\partial}{\partial t} m_0 + \frac{\partial}{\partial x} m_1 = 0 \tag{7}$$

$$\frac{\partial}{\partial t} m_1 + \frac{\partial}{\partial x} m_2 = \left(-\frac{\partial V}{\partial x} + R * E \right) m_0 \tag{8}$$

$$\cdots + \ldots = \ldots$$

$$\frac{\partial}{\partial t} m_k + \frac{\partial}{\partial x} m_{k+1} =$$
$$\left(-\frac{\partial V}{\partial x} + R * E \right) k m_{k-1} \tag{9}$$

$$\cdots + \ldots = \ldots$$

$$\frac{\partial}{\partial t} m_{2N_{\text{max}}-1} + \frac{\partial}{\partial x} m_{2N_{\text{max}}} =$$
$$\left(-\frac{\partial V}{\partial x} + R * E \right) (2N_{\text{max}} - 1) m_{2N_{\text{max}}-2} \tag{10}$$

where $m_0 = m_0(m_1, \ldots m_{2N})$ and the form of the closure depends on how many phases are in the solution [6]. We have identified ρ in (1) and (2) with m_0 of the moment formulation since we want the density to contain contributions from all of the values in the multi-valued solution, i.e.,

$$m_0(x,t) = \sum_{k=1}^{N(x,t)} \rho_k(x,t). \tag{11}$$

At the outset of a calculation one assumes a maximum number of phases in the solution N_{max}, and solves $2N_{\text{max}}$ moment equations. When the number of phases in the solution is less than N_{max} the extra moment equations are redundant. For example, when the number of phases is $N = 1$, then the closure relation is $m_0 = m_1^2/m_2$ and Eqs. (1)–(4) are recovered.

We solve the system as a boundary value problem with boundary values

$$V(0,t) = V_a \cos \omega t$$
$$E(0,t) = 0$$
$$m_0(0,t) = m_1(0,t) = \cdots = m_{2N_{\text{max}}}(0,t) = 1$$

where V_a is computed from input power as shown in Appendix A. In this paper we set $N_{\text{max}} = 3$ and the indicator functions $\varphi_1(x,t)$ and $\varphi_2(x,t)$ [6], which are special combinations of the moments that are related to the closure relations, track the number of phases in the solution.

The moment equations are solved with a first order kinetic scheme [6]; Eq. (6) is solved as in [6]; Eq. (5) is decomposed spectrally in t with an FFT, and stepped in x using a fourth order Runge-Kutta scheme. All convolutions are calculated in the frequency domain using an FFT, a multiplication by the frequency dependent function, and then an inverse FFT.

For parameters of interest we have shown that the linearization of Eqs. (5), (7), and (8) [with $R = 0$], using the single phase closure relation $m_0 = m_1^2/m_2$, form a hyperbolic system. In contrast to the klystron [6], however, the system is linearly unstable when $R \neq 0$ and (6) is coupled in. Ideally a numerical method accounting for this hyperbolicity would be used, but in lieu of such a new method we have found that solving Eq. (5) as described above produces acceptable results.

III. RESULTS AND DISCUSSION

In this section we present results from solving the moment system (5)–(10) for the X-WING TWT [17, 18], and compare the results to the Lagrangian method given in Appendix B. We use X-WING parameters at $f_1 = 4$ GHz which may be found in [18], and set $P_{\text{in}} = 4$ dBm.

Since TWTs tend to be very wide bandwidth amplifiers, harmonic generation in the beam current results in harmonics in the circuit field, and these harmonics are very important in practical applications. However, accounting for harmonics in circuit voltage and space charge field distorts phase space and destroys the classical "hook-like" structures and electron trapping widely known in electron beam devices. Therefore, to maintain as "clean" a phase space as possible for comparing the Eulerian and Lagrangian techniques, we arrange for our models to account only for the fundamental input frequency. In the Eulerian calculation this is accomplished by using the frequency dependent parameters $\delta(\omega - \omega_1)\tilde{C}^3(\omega)$ and $\delta(\omega - \omega_1)\tilde{R}(\omega)$ in the filtering operations. Furthermore, $\tilde{v}_{\text{ph}}(\omega)$ is set to the constant value of $\tilde{v}_{\text{ph}}(\omega_1)$. For the Lagrangian calculation the Fourier series representations (B3) and (B4) are restricted to the fundamental frequency only.

In Figs. 2 and 3 we show the beam velocity and beam density results from the Lagrangian calculation for the entire length of the TWT at an instant of time, as well as an expanded view of the multi-phase region. As one can see, the density becomes delta-function like concentrations at points where the velocity becomes multi-valued. In subsequent figures we will focus on comparing the methods in the multi-phase region.

In Fig. 4 we show the circuit voltage predicted by the Eulerian and Lagrangian calculations. Generally the circuit voltages are seen to be in good agreement even though, as will be seen in following figures, the velocity and density details predicted by the two techniques do not agree precisely. This is due to the fact that we have prevented density harmonics from producing voltage harmonics, and hence prevented by filtering any detailed fine structure of the beam evolution to manifest in the voltage.

For a better view of the detailed phase space and density structures in the multi-phase region predicted by the two methods we plot expanded views of the velocity and density in Figs. 5–7. The reader is referred to [5, 6] for
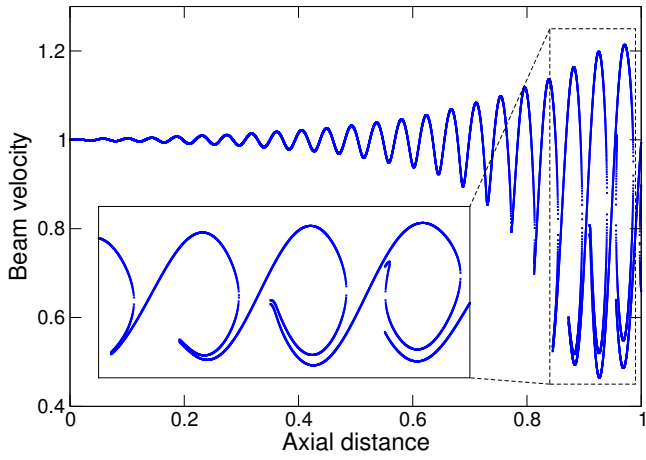
FIG. 2: (Color online) Beam velocity versus axial distance predicted by the Lagrangian method.
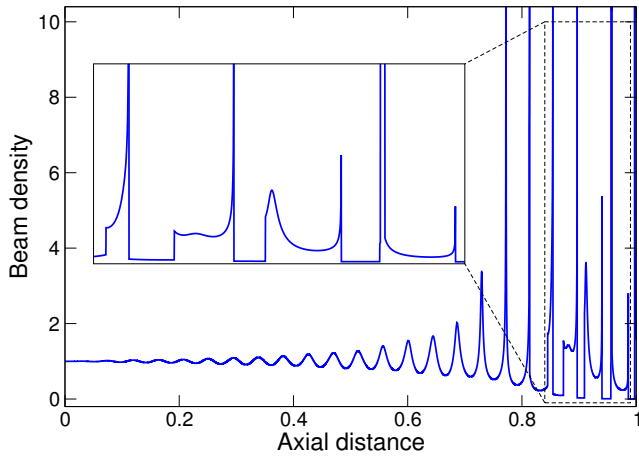

FIG. 3: (Color online) Beam density versus axial distance predicted by the Lagrangian method.
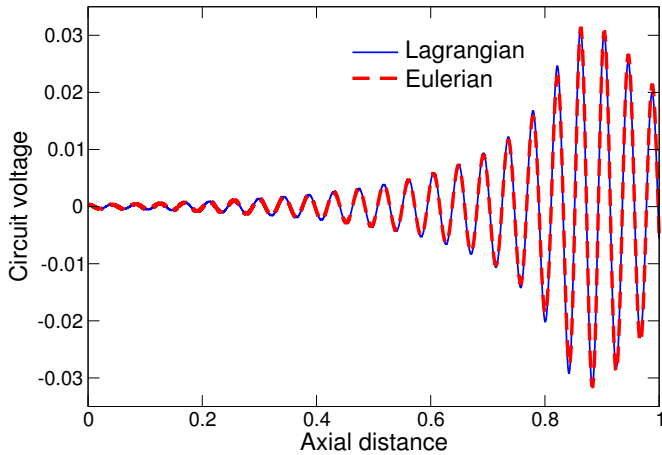

FIG. 4: (Color online) Circuit voltage versus axial distance for Eulerian and Lagrangian calculations.

details on how one computes the multi-phased velocity from the moments. The multi-phase density, i.e., the density accounting for the superposition of the individual densities, is given by m_0 [see (11)], and the density for the Lagrangian calculation is obtained from Eq. (B9).
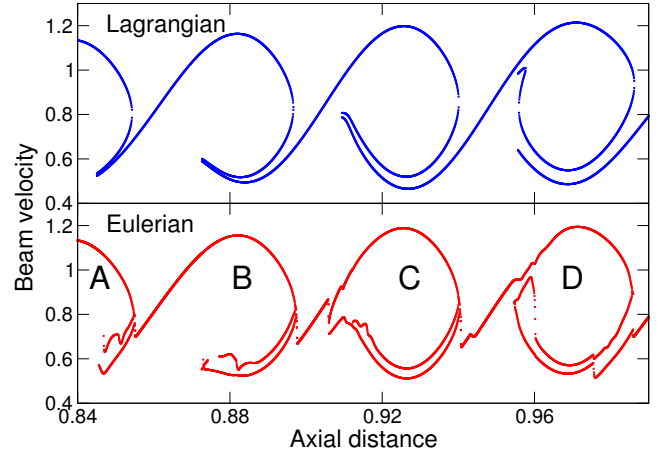

FIG. 5: (Color online) Expanded view of velocity comparing predictions of Eulerian and Lagrangian calculations.
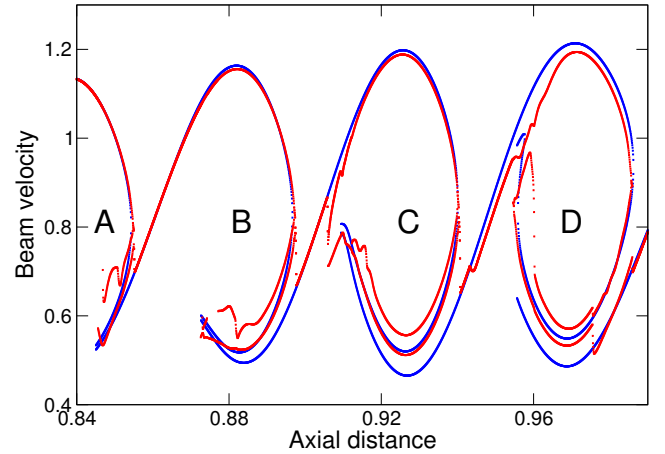

FIG. 6: (Color online) Expanded view of velocity overlaying predictions of Eulerian and Lagrangian calculations.

There are four multi-phased regions, labeled A–D in Figs. 5 and 6. The multi-phase technique properly predicts three phases for a majority of the multi-phase regions, although the quantitative values differ somewhat between the methods. Reasons for the discrepancies are due to the numerical difficulties associated with solving the moment equations (rather than the validity of the moment equations). The moment equations are a weakly hyperbolic system with discontinuous fluxes and density concentrations at phase boundaries. Currently the shock capturing methods often used for solving hyperbolic systems have not produced high quality results for the moment systems [21].
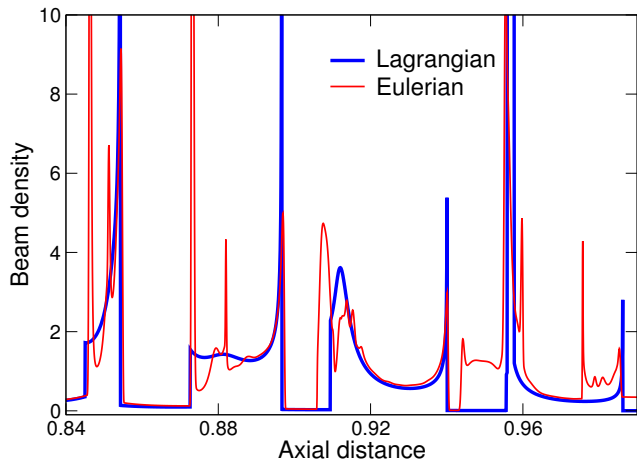
FIG. 7: (Color online) Expanded view of density comparing predictions of Eulerian and Lagrangian calculations.

The fact that density singularities coincide with the multi-phase boundaries can be verified for the respective methods. For regions A and B the location of these singularities matches between the methods. In regions C and D the agreement on the location of the left side singularity is not as good. Differences can again be attributed to the numerical methods used for the moment equations. Lastly, note that the Eulerian calculation predicts additional density singularities not present in the Lagrangian calculation. These "artificial" density singularities appear when the velocity changes from single valued to multi-valued, where the flux becomes discontinuous and singular. Due to the hyperbolic nature of the equations this discrepancy will not disappear, rather it will be carried along with the wave. This is one of the main numerical difficulties associated with the approach of the moment equations, as already pointed out in [5, 21].

In region D the Lagrangian calculation shows that there is a very small sub-region where there are five values in the velocity solution. We have set $N_{\max} = 3$ so the Eulerian calculation can compute at most three phases in this region. To run the calculation with $N_{\max} = 5$ one needs either to derive closure relations for m_0 for $N = 4$ and $N = 5$, or to implement numerical methods for solving the closures. Analytic closure relations have been derived up to $N = 5$ for initial value problems [22], but they have not been derived for boundary value problems.

In general to get reasonable agreement between the methods we have found that for the Eulerian calculation the space and time steps need a high degree of resolution. In the Eulerian calculations we used a step size of $h = 10^{-5}$ for a normalized length of 1.0, and $\lambda = k/h = 2.2$. With larger h multi-phase behavior is still predicted, but the exponential growth rate of the circuit voltage is under predicted and the density singularities are, of course, not as well resolved. The threshold values for the indicator functions [6] φ_1 and φ_2, i.e., values above

which the indicator functions are considered nonzero, are $\delta_1 = 10^{-4}$ and $\delta_2 = 5 \times 10^{-9}$. These values were arrived at by trial and error using results from the Lagrangian calculation to predict how many phases were expected in the Eulerian solution. In particular, since we knew not to expect any regions with two phases we set δ_1 to a relatively large number.

For the Lagrangian calculations we used $h = 6.67 \times 10^{-5}$ and $50,000$ rays ("disks") in one period of (normalized) $4\,\mathrm{GHz}$, compared to 2355 time steps for one period in the Eulerian calculation. The large number of rays is used to obtain good resolution on the phase space and density plots. With these parameters both methods take roughly one hour of computation time on a modern Gnu/Linux PC.

IV. CONCLUSIONS

The TWT has been used as a means to study the beam-plasma instability [14], and hence it provides a useful prototype wherein to study the potential application of a new Eulerian method for computing multi-valued solutions to general plasma instabilities. We apply the new method to the TWT, and compare the results to Lagrangian calculations.

We compare the methods for a case that develops significant multi-phase content in the solution. The two methods show good qualitative agreement regarding the number of phases in the solution and the location of density singularities, while they differ somewhat in quantitative predictions of the solutions. These differences are due to the fact that we still do not have a good numerical method for the moment system which is weakly hyperbolic with discontinuous fluxes at phase boundaries.

For the calculations in this paper we restrict the harmonic content of the circuit voltage and space charge electric field so that the phase space is "clean" and comparisons between the methods are easily made. We have performed calculations for the case of this paper accounting for ten voltage and space charge field harmonics. The results show that, similar to the results shown in this paper, the circuit voltages agree while the multi-valued velocity and density solutions agree qualitatively in structure, but have quantitative differences that are due to the immaturity of the numerical methods.

APPENDIX A: NORMALIZATION AND VLASOV EQUATION

The unnormalized TWT equations are

$$\frac{\partial V}{\partial x} + \frac{1}{v_{\text{ph}}} * \frac{\partial V}{\partial t} = \frac{KA}{2} * \frac{\partial \rho}{\partial t} \qquad (A1)$$

$$\frac{\partial E}{\partial x} = \frac{\rho - \rho_0}{\epsilon_0} \qquad (A2)$$

$$\frac{\partial \rho}{\partial t} + \frac{\partial}{\partial x}(\rho u) = 0 \qquad (A3)$$

$$\frac{\partial}{\partial t}(\rho u) + \frac{\partial}{\partial x}(\rho u^2) = \frac{e}{m_e}\rho\left(-\frac{\partial V}{\partial x} + R * E\right). \quad (A4)$$

In addition to the parameters given in Sec. II, A is the electron beam area, K is the inverse Fourier transform of the frequency dependent interaction impedance $\tilde{K}(\omega)$, ρ_0 is the dc beam charge density, and ϵ_0, e, m_e are free space permittivity, electron charge, and electron mass respectively.

To normalize (A1)–(A4) we first introduce the characteristic time

$$T = \frac{L}{u_0} \qquad (A5)$$

where L is the TWT length and u_0 is the dc beam velocity, and then define independent coordinates

$$\hat{x} = \frac{x}{L} \quad \hat{t} = \frac{t}{T}. \qquad (A6)$$

Define the normalized dependent variables

$$\hat{V} = \frac{e}{m_e u_0^2} V, \quad \hat{E} = \frac{\epsilon_0}{L\rho_0} E, \quad \hat{u} = \frac{u}{u_0}, \quad \hat{\rho} = \frac{\rho}{\rho_0},$$

where

$$u_0 = \sqrt{\frac{2eV_0}{m_e}}, \quad \rho_0 = \frac{I_0}{u_0 A},$$

and parameters

$$\hat{v}_{\text{ph}} = \frac{v_{\text{ph}}}{u_0}, \quad \hat{R} = R\frac{eL^2\rho_0}{m_e u_0^2 \epsilon_0}, \quad C^3 = \frac{KI_0}{4V_0},$$

where V_0, I_0 are beam voltage and current, respectively. These definitions lead to the normalized TWT equations (1)–(4).

Given input power P_{in} the voltage amplitude is given by

$$V_a = \frac{\sqrt{8P_{\text{in}}K}}{V_0}, \qquad (A7)$$

where a factor of $2/V_0$ takes care of the normalization.

For the Vlasov equation

$$\frac{\partial f}{\partial t} + v\frac{\partial f}{\partial x} + \frac{e}{m_e}\left(-\frac{\partial V}{\partial x} + R * E\right)\frac{\partial f}{\partial v} = 0 \qquad (A8)$$

use the normalizations above, plus

$$\hat{v} = \frac{v}{u_0}, \qquad \hat{f} = f\frac{eu_0}{\rho_0},$$

and take the kth velocity moment of the Vlasov equation (in normalized variables)

$$\frac{\partial}{\partial t}\int fv^k dv + \frac{\partial}{\partial x}\int fv^{k+1} dv$$
$$= -\left(-\frac{\partial V}{\partial x} + R * E\right)\int \frac{\partial f}{\partial v}v^k dv. \qquad (A9)$$

Integrate the last term by parts and define

$$m_k \equiv \int fv^k dv \qquad (A10)$$

to get

$$\frac{\partial}{\partial t}m_k + \frac{\partial}{\partial x}m_{k+1}$$
$$= \left(-\frac{\partial V}{\partial x} + R * E\right)km_{k-1}. \qquad (A11)$$

APPENDIX B: LAGRANGIAN FORMULATION

For solving in Lagrangian coordinates we need the Fourier coefficients of the charge density ρ

$$\hat{\rho}_\ell(x) = \frac{\omega_0}{2\pi}\int_0^{2\pi/\omega_0} \rho(x,t)\,e^{-i\ell\omega_0 t}\,dt \qquad (B1)$$

$$= \frac{\omega_0}{2\pi}\int_0^{2\pi/\omega_0} \frac{I^0(t_0)}{\hat{u}(x,t_0)}e^{-i\ell\omega_0\hat{t}(x,t_0)}\,dt_0. \quad (B2)$$

Equation (B2) is the Fourier coefficient of ρ written in Lagrangian coordinates. Using a Fourier representation of $V(x,t)$, $E(x,t)$, i.e.,

$$V(x,t) = \sum_{\ell=-\infty}^{\infty} \hat{V}_\ell(x)e^{i\ell\omega_0 t}, \qquad (B3)$$

$$E(x,t) = \sum_{\ell=-\infty}^{\infty} \hat{E}_\ell(x)e^{i\ell\omega_0 t}, \qquad (B4)$$

and a Fourier representation of $\rho(x,t)$ we get from (1) and (2)

$$\frac{d\tilde{V}_\ell}{dx} = i\ell\omega_0\left(-\frac{\tilde{V}_\ell}{\tilde{v}_{\text{ph}\ell}} + \hat{C}_\ell^3\tilde{\rho}_\ell\right), \qquad \ell \neq 0 \quad (B5)$$

$$\frac{d\tilde{E}_\ell}{dx} = \tilde{\rho}_\ell, \qquad \ell \neq 0. \qquad (B6)$$

The characteristics $\hat{t}(x,t_0), \hat{u}(x,t_0)$ are solved from

$$\frac{\partial \hat{t}}{\partial x} = \frac{1}{\hat{u}} \qquad (B7)$$

$$\frac{\partial \hat{u}}{\partial x} = \frac{1}{\hat{u}}\sum_{\ell=-\infty}^{\infty}\left[i\ell\omega_0\left(\frac{\hat{V}_\ell}{\hat{v}_{\text{ph}\ell}} - \hat{C}_\ell^3\tilde{\rho}_\ell\right) + \hat{R}_\ell\hat{E}_\ell\right]e^{i\ell\omega_0\hat{t}}. \qquad (B8)$$

We solve Eqs. (B5)–(B8) with a fourth order Runge-Kutta scheme, and approximate the Fourier series with a finite number of frequencies.

The beam charge density shown in Figs. 3 and Fig. 7 is solved from the Lagrangian continuity equation

$$\rho(x,t) \;=\; \sum_{\{t_0 : t = \hat{t}(x,t_0)\}} \frac{1}{\hat{u}\left|\frac{\partial \hat{t}}{\partial t_0}\right|} \qquad (B9)$$

where the sum accounts for all fluid elements t_0 arriving at (x,t). Equation (B9) was also used in deriving Eq. (B2).

[1] G. Whitham, F.R.S., *Linear and Nonlinear Waves* (Wiley, New York, 1974).
[2] Y. Brenier, and L. Corrias, Ann. Inst. Henri Poincaré **15(2)**, 169 (1998).
[3] B. Engquist, and O. Runborg, J. Comp. Appl. Math. **74**, 175 (1996).
[4] L. Gosse, J. Comp. Phys. **180(1)**, 155 (2002).
[5] S. Jin and X. Li, Physica D **182**, 46 (2003).
[6] X. Li, J. Wöhlbier, S. Jin, and J. Booske, Phys. Rev. E **70** (2004), article 016502.
[7] J. Dawson, Physical Review **113**, 383 (1959).
[8] J. Albritton and P. Koch, Phys. Fluids **18**, 1136 (1975).
[9] W. Kruer, Physica Scripta **T30**, 5 (1990).
[10] W. Mori and T. Katsouleas, Physica Scripta **T30**, 127 (1990).
[11] J. Wang, G. Payne, and D. Nicholson, Phys. Fluids B **4**, 1432 (1992).
[12] A. C.-L. Chian, Phys. Rev. A **39**, 2561 (1989).
[13] A. Nordsieck, Proc. IRE **41**, 630 (1953).
[14] G. Dimonte and J. Malmberg, Phys. Fluids **21**, 1188 (1978).
[15] A. Klimas and J. Cooper, Phys. Fluids **26**, 478 (1983).
[16] S. Jin and J. Wöhlbier, (To be submitted) (2005).
[17] M. Converse, Ph.D. thesis, University of Wisconsin–Madison (2003).
[18] M. Converse, J. Booske, and S. Hagness, IEEE Trans. Plasma Sci. **32**, 1040 (2004).
[19] J. Pierce, *Traveling Wave Tubes* (Van Nostrand, Princeton, N.J., 1950).
[20] A. Gilmour, Jr., *Principles of Traveling Wave Tubes* (Artech House, Boston, 1994).
[21] L. Gosse, S. Jin, and X.T. Li, Math. Models Methods Appl. Sci. **13**, 1689 (2003).
[22] X. Li, Ph.D. thesis, University of Wisconsin–Madison (2002).